Smart Mater. Struct. **16** (2007) 2605–2620 doi:10.1088/0964-1726/16/6/065

Topology optimization design of functionally graded bimorph-type piezoelectric actuators

Ronny C Carbonari[1], **Emílio C N Silva**[1] **and Glaucio H Paulino**[2]

[1] Department of Mechatronics and Mechanical Systems Engineering, Escola Politécnica da Universidade de São Paulo, Avenida Prof. Mello Moraes, 2231, 05508-900, São Paulo, SP, Brazil

[2] Newmark Laboratory, Department of Civil and Environmental Engineering, University of Illinois at Urbana-Champaign, 205 North Mathews Avenue, Urbana, IL 61801, USA

E-mail: ronny@usp.br, ecnsilva@usp.br and paulino@uiuc.edu

Received 5 February 2007, in final form 5 August 2007
Published 1 November 2007
Online at stacks.iop.org/SMS/16/2605

Abstract

The concept of a functionally graded material (FGM) is useful for engineering advanced piezoelectric actuators. For instance, it can lead to locally improved properties, and to increased lifetime of bimorph piezoelectric actuators. By selectively grading the elastic, piezoelectric, and/or dielectric properties along the thickness of a piezoceramic, the resulting gradation of electromechanical properties influences the behavior and performance of piezoactuators. In this work, topology optimization is applied to find the optimum gradation and polarization sign variation in piezoceramic domains in order to improve actuator performance measured in terms of selected output displacements. A bimorph-type actuator is emphasized, which is designed by maximizing the output displacement or output force at selected location(s) (e.g. the tip of the actuator). The numerical discretization is based on the graded finite element concept such that a continuum approximation of material distribution, which is appropriate to model FGMs, is achieved. The present results consider two-dimensional models with a plane-strain assumption. The material gradation plays an important role in improving the actuator performance when distributing piezoelectric (PZT5A) and non-piezoelectric (gold) materials in the design domain; however, the performance is not improved when distributing two types of similar piezoelectric material. In both cases, the polarization sign change did not play a significant role in the results. However, the optimizer always finds a solution with opposite polarization (as expected).

(Some figures in this article are in colour only in the electronic version)

1. Introduction

Piezoelectric microdevices have a wide range of applications in precision mechanics, nanopositioning and micromanipulation apparatus. Functionally graded materials (FGMs) are special materials that possess continuously graded properties and are characterized by spatially varying microstructures created by nonuniform distributions of the reinforcement phase as well as by interchanging the role of reinforcement and matrix (base) materials in a continuous manner (Suresh and Mortensen 1988, Miyamoto *et al* 1999). The smooth variation of properties may offer advantages such as increased bonding strength and local control of the electrical field. Recently, this concept has been explored in piezoelectric materials to improve the properties and to increase the lifetime of piezoelectric actuators (Ballato *et al* 2001, Zhu and Meng 1995, Qiu *et al* 2003). These actuators have attracted significant attention due to their simplicity, usefulness, and reliability. Usually, elastic,

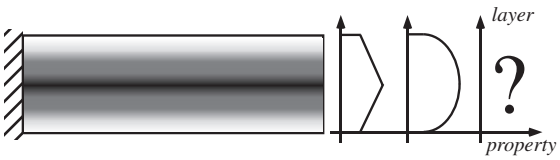

Figure 1. Finding the optimum gradation variation in FGM piezoceramics.

piezoelectric, and dielectric properties are graded along the thickness of an FGM bimorph piezoactuator (see figure 1). This gradation can be achieved by stacking piezoelectric composites of different compositions on top of each other (Zhu and Meng 1995, Qiu *et al* 2003, Chen *et al* 2003). Each lamina can be composed by a piezoelectric material or a composite made of both piezoelectric material and non-piezoelectric material. Due to their relevance, several studies have been conducted on FGM actuators (Zhu and Meng 1995, Zhifei 2002, Ying and Zhifei 2005, Elka *et al* 2004, Shi and Chen 2004, Almajid *et al* 2001, Taya *et al* 2003). Another example of a piezoactuator that can take advantage of the FGM concept is the rainbow-type actuator (Haertling 1994). Previous studies (Almajid *et al* 2001, Taya *et al* 2003) have shown that the gradation of piezoceramic properties can have a significant influence on the performance of bimorph piezoactuators, such as generated output displacements. This suggests that optimization techniques can be applied to take advantage of selective property gradation variation in order to improve FGM piezoactuator performance.

Topology optimization is a powerful structural optimization method that seeks an optimal structural topology design by determining which points of space should be solid and which points should be void (i.e. no material) inside a given domain (Sigmund 2000). However, the binary (0–1) design is an ill-posed problem and a typical way to seek a solution consists of relaxing the problem by defining a material model that allows for intermediate (composite) property values (Torquato 2002). In this sense, the relaxation yields a continuous material design problem that no longer involves a discernible connectivity. Typically, it is an improperly formulated (ill-posed) topology optimization problem for which no optimum solution exists (0–1 design). A feasible topology solution can be obtained by applying penalization coefficients to the material model to recover the 0–1 design (and thus, a discernible connectivity), and some gradient control of material distribution, such as a filter (Bendsøe and Sigmund 2003).

The relaxed problem is strongly related to the FGM design problem, which essentially seeks a continuous transition of material properties. The 0–1 design problem needs complexity control (such as a filter) and does not admit intermediate values of design variables, while the FGM design problem does not need complexity control and does admit solutions with intermediate values of the material field. This approach is explored in the present paper.

In this work, topology optimization is applied to find the optimum gradation and polarization sign variation in FGM piezoceramics to achieve improved piezoactuator performance measured in terms of output displacements. A bimorph-type actuator design is considered. Accordingly, the optimization problem is posed as finding the optimized piezoelectric property gradation and polarization sign variation (see figure 1) that maximizes the output displacement or output force at the tip of a bimorph actuator while minimizing the effects of movement coupling. The optimization algorithm combines the finite element method with sequential linear programming (SLP). The finite element method is based on the graded finite element concept where the properties change smoothly inside the element. The material model is implemented based on both the solid isotropic material with penalization (SIMP) model (Bendsøe and Sigmund 2003) and the continuum approximation of material distribution (CAMD) (Matsui and Terada 2004) where fictitious densities are interpolated at each finite element. This approach provides a continuum material distribution, which is appropriate to model FGMs (Kim and Paulino 2002). The present results consider gradation between either two different piezoceramic properties or a non-piezoelectric (such as gold) and a piezoelectric material, and consider two-dimensional models with a plane-strain assumption.

This paper is organized as follows. In section 2, a brief introduction to the numerical modeling of FGM piezoceramics, considering graded finite elements, is presented. In section 3, the continuous topology optimization method together with the adopted material model, and also the problem formulation of FGM piezoactuator design, are described. In section 4 and appendix A, the numerical implementation and the sensitivity analysis for the design problem, respectively, are discussed. In section 5, a projection technique for material gradation control is given. In section 6, the design of an optimized FGM bimorph type piezoactuator is provided. Finally, in section 7, some conclusions are inferred.

2. Functionally graded piezoelectric finite element model

The FGM piezoelectric actuators designed here operate in quasi-static or low-frequency environments where inertia effects can be ignored. The weak formulation of the equilibrium equations of the piezoelectric medium considering linear piezoelectricity is mature and it is given by Lerch (1990)

$$\begin{aligned}
&\int_\Omega \boldsymbol{\varepsilon}(\mathbf{u})^{\mathrm{t}}\mathbf{c}^E\boldsymbol{\varepsilon}(\mathbf{v})\,\mathrm{d}\Omega + \int_\Omega (\nabla\phi)^{\mathrm{t}}\mathbf{e}^{\mathrm{t}}\boldsymbol{\varepsilon}(\mathbf{v})\,\mathrm{d}\Omega = \int_{\Gamma_{\mathbf{t}}} \mathbf{t}\cdot\mathbf{v}\,\mathrm{d}\Gamma \\
&\int_\Omega \boldsymbol{\varepsilon}(\mathbf{u})^{\mathrm{t}}\mathbf{e}\nabla\varphi\,\mathrm{d}\Omega - \int_\Omega (\nabla\phi)^{\mathrm{t}}\boldsymbol{\epsilon}^S\nabla\varphi\,\mathrm{d}\Omega = \int_{\Gamma_d} d\varphi\,\mathrm{d}\Gamma \qquad (1)\\
&\qquad \text{for } \mathbf{u},\phi \in V \qquad \text{and} \qquad \forall\mathbf{v},\forall\varphi \in V
\end{aligned}$$

where

$$\mathbf{t} = \boldsymbol{\sigma}\cdot\mathbf{n}; \qquad d = \mathbf{D}\cdot\mathbf{n} \qquad (2)$$

are the mechanical traction and electrical charge, respectively, $\mathbf{n}$ is the normal vector to the surface,

$$V = \{\mathbf{v} = v_i\bar{\mathbf{e}}_i, \varphi \text{ with } \mathbf{v} = 0 \text{ on } \Gamma_{\mathbf{u}} \text{ and } \varphi = 0 \text{ on } \Gamma_\phi, i = 1 \text{ or } 3\},$$

Ω is the domain of the medium (it may contain piezoelectric and non-piezoelectric materials), and ∇ is the gradient operator. The superscript 't' denotes transpose, $\mathbf{v}$ and φ are virtual displacements and electric potential, respectively, $\mathbf{u}$ is the displacement field, and ϕ is the electric potential in the

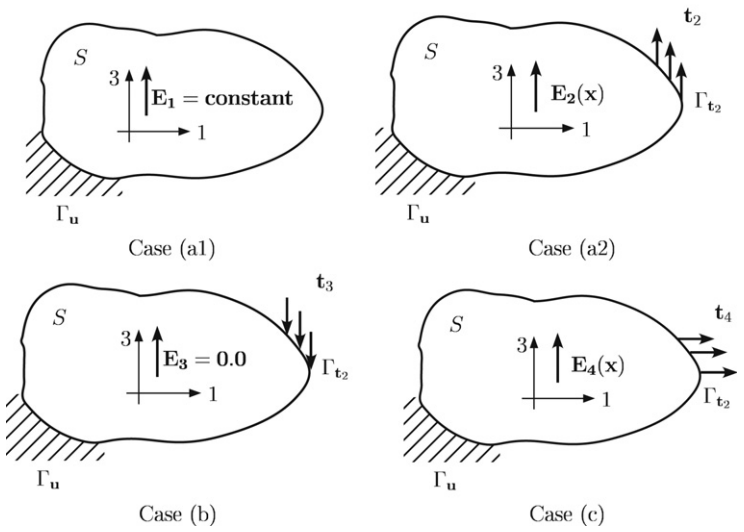

Figure 2. General load cases used for calculation of the mean transduction and coupling constraint (cases a1, a2, and c, respectively), and mean compliance (case b). Here, $\mathbf{E}_i = -\nabla\phi_i$ denotes the electrical field associated with load case i.

piezoelectric medium. The index i assumes a value 1 or 3 because the problem is considered in the 1–3 plane. The piezoceramic is polarized in the local 3-direction (see figure 2).

The matrix formulation of the equilibrium equations for the piezoelectric medium is given by Naillon *et al* (1983)

$$\begin{bmatrix} \mathbf{K}_{uu} & \mathbf{K}_{u\phi} \\ \mathbf{K}_{u\phi}^{\mathrm{t}} & -\mathbf{K}_{\phi\phi} \end{bmatrix} \begin{Bmatrix} \mathbf{U} \\ \mathbf{\Phi} \end{Bmatrix} = \begin{Bmatrix} \mathbf{F} \\ \mathbf{Q} \end{Bmatrix} \Longrightarrow [\mathcal{K}]\{\mathcal{U}\} = \{\mathcal{Q}\} \qquad (3)$$

where $\mathbf{K}_{uu}$, $\mathbf{K}_{u\phi}$, and $\mathbf{K}_{\phi\phi}$ denote the stiffness, piezoelectric, and dielectric matrices, respectively, and $\mathbf{F}$, $\mathbf{Q}$, $\mathbf{U}$, and $\mathbf{\Phi}$ are the nodal mechanical force, nodal electrical charge, nodal displacements, and nodal electric potential vectors, respectively. However, in the case of FGM piezoceramics the properties change continuously inside the piezoceramic domain, which means that they can be described by some continuous function of position $\mathbf{x}$ in the domain, that is,

$$\mathbf{c}^E = \mathbf{c}^E(\mathbf{x}); \qquad \mathbf{e} = \mathbf{e}(\mathbf{x}); \qquad \boldsymbol{\epsilon}^S = \boldsymbol{\epsilon}^S(\mathbf{x}). \qquad (4)$$

From the mathematical definitions of $\mathbf{K}_{uu}$, $\mathbf{K}_{u\phi}$, and $\mathbf{K}_{\phi\phi}$, these material properties must remain inside the matrix integrals and be integrated together by using the graded finite element concept (Kim and Paulino 2002) where properties are continuously interpolated inside each finite element based on property values at each finite element node. An attempt to approximate the continuous change of material properties by a stepwise function where a property value is assigned for each finite element may result in less accurate results with undesirable discontinuities of the stress and strain fields (Kim and Paulino 2002).

When a non-piezoelectric conductor material and a piezoceramic material are distributed in the piezoceramic domain, the electrode positions are not known *a priori*, as discussed below. Therefore, the electrical excitations are given by an applied electric field ($\nabla\phi$ = constant), and thus, equation (1) becomes (Carbonari *et al* 2007),

$$\begin{aligned} &\int_\Omega \boldsymbol{\varepsilon}(\mathbf{u})^{\mathrm{t}}\mathbf{c}^E\boldsymbol{\varepsilon}(\mathbf{v})\,\mathrm{d}\Omega = \int_{\Gamma_\mathbf{t}} \mathbf{t}\cdot\mathbf{v}\,\mathrm{d}\Gamma - \int_\Omega (\nabla\phi)^{\mathrm{t}}\mathbf{e}^{\mathrm{t}}\boldsymbol{\varepsilon}(\mathbf{v})\,\mathrm{d}\Omega \\ &\int_\Omega \boldsymbol{\varepsilon}(\mathbf{u})^{\mathrm{t}}\mathbf{e}\nabla\varphi\,\mathrm{d}\Omega = \int_\Omega (\nabla\phi)^{\mathrm{t}}\boldsymbol{\epsilon}^S\nabla\varphi\,\mathrm{d}\Omega + \int_{\Gamma_d} d\varphi\,\mathrm{d}\Gamma \qquad (5) \\ &\text{for } \mathbf{u}, \phi \in V \qquad \text{and} \qquad \forall\mathbf{v}, \forall\varphi \in V. \end{aligned}$$

In this case, all electrical degrees of freedom are prescribed in the FE problem, and equation (3) is rewritten as

$$[\mathbf{K}_{uu}]\{\mathbf{U}\} = \{\mathbf{F}\} - \left[\mathbf{K}_{u\phi}\right]\{\mathbf{\Phi}\} \qquad (6)$$

$$\left[\mathbf{K}_{u\phi}^{\mathrm{t}}\right]\{\mathbf{U}\} = \{\mathbf{Q}\} + \left[\mathbf{K}_{\phi\phi}\right]\{\mathbf{\Phi}\} \qquad (7)$$

as $\{\mathbf{\Phi}\}$ is prescribed. Thus, the mechanical and electrical problems are decoupled, and only equation (6) needs to be directly solved. Essentially, the optimization problem is based on the mechanical problem and, as a consequence, the dielectric properties do not influence the design.

3. Topology optimization

The basic topology optimization framework used in this work is based on the formulation described in detail by Carbonari *et al* (2007), which is extended here to the FGM piezoelectric actuators. It is a continuous topology optimization formulation where a continuum distribution of the design variable inside the finite element is considered through interpolation by means of a continuous function. In this case, the design variables related to the material distribution are defined for each node instead of each finite element as usual. This formulation, known as the 'Continuous Approximation of Material Distribution' or CAMD (Matsui and Terada 2004), appears to be robust and also fully compatible with the FGM concept.

We are interested in a continuous distribution of piezoelectric materials in the design domain. Additionally, the polarization sign in the piezoelectric domain must be taken into account to increase design flexibility. This can be achieved by defining a design variable ρ_1 related to the sign of the

piezoelectric property **e**, and thus, to the polarization sign of the piezoelectric material (Carbonari *et al* 2007). As shown later, the inclusion of the polarization sign in the optimization process significantly improves the design and performance of the final actuator. The following adopted material models are based on a simple extension of the traditional SIMP model (Bendsøe and Sigmund 2003):

$$\mathbf{C}^H = \rho_1 \mathbf{C}_1 + (1 - \rho_1)\mathbf{C}_2 \tag{8}$$

$$\mathbf{e}^H = (2\rho_2 - 1)^{p_e}[\rho_1 \mathbf{e}_1 + (1 - \rho_1)\mathbf{e}_2] \tag{9}$$

where ρ_1 is a pseudo-density function describing the amount of material at each point of the domain, which is given by

- $\rho_1 = 1.0$ denotes piezoelectric material type 1;
- $\rho_1 = 0.0$ denotes piezoelectric material type 2.

The design variables can assume different values at each finite element node. The mixture material parameters $\mathbf{C}^H$ and $\mathbf{e}^H$ are stiffness and piezoelectric tensor properties, respectively. The tensors $\mathbf{C}_i$ and $\mathbf{e}_i$ are related to the stiffness and piezoelectric properties for piezoelectric material type i ($i = 1, 2$), respectively. These are the properties of basic materials that are distributed in the piezoceramic domain to form the FGM piezocomposite.

The design variable ρ_2 is related to the polarization sign in the piezoceramic domain. Its value should tend to zero or unity, indicating that the polarization is either negative or positive, respectively. The penalization factor p_e is an odd number that is applied to avoid intermediate values of ρ_2 as we are interested only in positive or negative polarization signs. Thus, the above material model allows the algorithm not only to optimize the material distribution but also to choose a suitable polarization (positive or negative) at each point (see equation (9)). In this work, we consider two signs for the polarization (negative or positive). For the bimorph-type actuator, the mechanical interaction between the two piezoceramic domains with opposite polarizations generate bending strains. The article by Chen and Roytburd (2007) discusses the influence of polarization on longitudinal strains (but not bending).

The dielectric properties are not considered because a constant electric field is applied to the design domain as electrical excitation. As explained in section 4, this approach decouples the electrical and mechanical problems eliminating the influence of dielectric properties in the optimization problem. Eventually, the piezoelectric material type 2 can be substituted by a non-piezoelectric material (elastic material, such as gold, for example), and in this case $\mathbf{e_2} = \mathbf{0}$. For a domain discretized into finite elements, equations (8) and (9) are considered for each element node, and the material properties inside each finite element are given by a function $\rho_1 = \rho_1(\mathbf{x})$, according to the CAMD concept, where $\mathbf{x}$ denotes the Cartesian coordinates. This formulation leads to a continuous distribution of material in the design domain which is ideal for the FGMs. Thus, by finding nodal values of the unknown ρ_1 function, we obtain (indirectly) the optimum material distribution functions, which are described by equation (4).

The theoretical formulation for piezoelectric actuator design optimization by topology optimization is briefly revisited here considering an electrical field excitation. The goal is to design a device that generates the maximum output displacement considering a fixed piezoceramic domain. However, in this work, the piezoceramic domain is not fixed and the piezoceramic electrodes are not known '*a priori*'. Thus, to address this problem, an electric field ($\mathbf{E}_i$) is applied to the domain as electrical excitation. Essentially, the objective function is defined in terms of generated output displacements for a certain applied electric field to the design domain. The mean transduction ($L_2(\mathbf{u}_1, \phi_1)$) concept is related to the electromechanical conversion represented by the displacement generated in region $\Gamma_{\mathbf{t}_2}$ in a specified direction due to an input electrical excitation in the medium. Thus, the larger $L_2(\mathbf{u}_1, \phi_1)$, the larger the displacement generated in this region in the $\mathbf{t}_2$-direction due to an applied electric field to the medium (in this work, $\mathbf{E}_1$ is prescribed). The mean transduction is given by Silva *et al* (2000)

$$L_2(\mathbf{u}_1, \phi_1) = \int_{\Gamma_{t_2}} \mathbf{t}_2 \mathbf{u}_1 \, \mathrm{d}\Gamma + \int_{\Gamma_{d_2}} d_2 \phi_1 \, \mathrm{d}\Gamma = \int_{\Gamma_{t_2}} \mathbf{t}_2 \mathbf{u}_1 \, \mathrm{d}\Gamma \tag{10}$$

and $d_2 = 0$ in this problem, where d_2 is the distributed electrical charge at the output displacement region associated with the load case shown in figure 2(a2). Therefore, the maximization of output displacement generated in a region $\Gamma_{\mathbf{t}_2}$ is obtained by maximizing the *mean transduction* quantity ($L_2(\mathbf{u}_1, \phi_1)$). The general load cases considered for calculation of mean transduction are shown in cases (a1) and (a2) of figure 2.

The piezoactuator must resist reaction forces generated (in region $\Gamma_{\mathbf{t}_2}$) by the body that the piezoactuator is trying to move or grab. Therefore, the mean compliance must be minimized to provide enough stiffness (see figure 2(b)). The mean compliance is calculated by considering the load case described in case (b) of figure 2, where traction $\mathbf{t}_3 = -\mathbf{t}_2$ is applied to region $\Gamma_{\mathbf{t}_2}$ and the electric field is kept null inside the medium ($\mathbf{E}_3 = 0$). Thus, it is given by Silva *et al* (2000)

$$L_3(\mathbf{u}_3, \phi_3) = \int_{\Gamma_{t_2}} \mathbf{t}_3 \mathbf{u}_3 \, \mathrm{d}\Gamma. \tag{11}$$

The displacement coupling constraint is obtained by minimizing the absolute value of the corresponding mean transduction related to the undesired generated displacement. This minimizes an undesired displacement generated when an electric field is applied. Therefore, the mean transduction $L_4(\mathbf{u}_1, \phi_1)$ related to the displacement normal to the desired displacement at $\Gamma_{\mathbf{t}_2}$ must be minimized (see figure 2(c)), and it is calculated by using equation (10), however, considering a traction $\mathbf{t}_4$, normal to $\mathbf{t}_2$, on region $\Gamma_{\mathbf{t}_2}$ (Carbonari *et al* 2005), as described in case (c) of figure 2.

To combine the mean transduction, mean compliance maximization, and coupling constraint minimization, a multi-objective function is constructed to find an appropriate optimal solution that can incorporate all design requirements. Thus, the following multi-objective function is proposed:

$$\mathcal{F}(\rho_1, \rho_2) = w * \ln[L_2(\mathbf{u}_1, \phi_1)] - \tfrac{1}{2}(1 - w) \ln\left[L_3(\mathbf{u}_3, \phi_3)^2 + \beta L_4(\mathbf{u}_1, \phi_1)^2\right] \tag{12}$$

where w and β are weight coefficients ($0 \leqslant w \leqslant 1$, $\beta > 0$). The value of the coefficient w allows control

of the contributions of mean transduction (equation (10)) in relation to mean compliance (equation (11)), and displacement coupling constraint function in the design. The value of the β coefficient allows control of the contribution of coupling constraint function. The final general optimization problem is defined as

$$
\begin{aligned}
&\text{Maximize:} && \mathcal{F}(\rho_1, \rho_2)\\
&\rho_1(\mathbf{x}),\ \rho_2(\mathbf{x})\\
&\text{subject to:} && \mathbf{t}_3 = -\mathbf{t}_2 \quad (\Gamma_{\mathbf{t}_3} = \Gamma_{\mathbf{t}_2})\\
&&& \mathbf{t}_4 \cdot \mathbf{t}_2 = 0 \quad (\Gamma_{\mathbf{t}_4} = \Gamma_{\mathbf{t}_2})\\
&&& a(\mathbf{u}_1, \mathbf{v}_1) + b(\phi_1, \mathbf{v}_1) = L_t(\mathbf{t}_1, \mathbf{v}_1)\\
&&& b(\varphi_1, \mathbf{u}_1) - c(\phi_1, \varphi_1) = L_d(d_1, \varphi_1)\\
&&& \text{for } \mathbf{u}_1, \phi_1 \in V_a \text{ and } \forall \mathbf{v}_1, \forall \varphi_1 \in V_a\\
&&& a(\mathbf{u}_2, \mathbf{v}_2) + b(\phi_2, \mathbf{v}_2) = L_t(\mathbf{t}_2, \mathbf{v}_2)\\
&&& b(\varphi_2, \mathbf{u}_2) - c(\phi_2, \varphi_2) = 0\\
&&& \text{for } \mathbf{u}_2, \phi_2 \in V_b \text{ and } \forall \mathbf{v}_2, \forall \varphi_2 \in V_b\\
&&& a(\mathbf{u}_3, \mathbf{v}_3) + b(\phi_3, \mathbf{v}_3) = L_t(\mathbf{t}_3, \mathbf{v}_3)\\
&&& b(\varphi_3, \mathbf{u}_3) - c(\phi_3, \varphi_3) = L_d(d_3, \varphi_3)\\
&&& \text{for } \mathbf{u}_3, \phi_3 \in V_c \text{ and } \forall \mathbf{v}_3, \forall \varphi_3 \in V_c\\
&&& a(\mathbf{u}_4, \mathbf{v}_4) + b(\phi_4, \mathbf{v}_4) = L_t(\mathbf{t}_4, \mathbf{v}_4)\\
&&& b(\varphi_4, \mathbf{u}_4) - c(\phi_4, \varphi_4) = 0\\
&&& \text{for } \mathbf{u}_4, \phi_4 \in V_b \text{ and } \forall \mathbf{v}_4, \forall \varphi_4 \in V_b\\
&&& 0 \leqslant \rho_1(\mathbf{x}) \leqslant 1\\
&&& 0 \leqslant \rho_2(\mathbf{x}) \leqslant 1\\
&&& \Theta(\rho_1) = \textstyle\int_S \rho_1 \,\mathrm{d}S - \Theta_1 \leqslant 0
\end{aligned}
\tag{13}
$$

where

$$
\begin{aligned}
a(\mathbf{u}, \mathbf{v}) &= \int_\Omega \boldsymbol{\varepsilon}(\mathbf{u})^{\mathrm{t}} \mathbf{c}^E \boldsymbol{\varepsilon}(\mathbf{v}) \,\mathrm{d}\Omega\\
(\phi, \mathbf{v}) &= \int_\Omega (\nabla\phi)^{\mathrm{t}} \mathbf{e}^{\mathrm{t}} \boldsymbol{\varepsilon}(\mathbf{v}) \,\mathrm{d}\Omega\\
c(\phi, \varphi) &= \int_\Omega (\nabla\phi)^{\mathrm{t}} \boldsymbol{\epsilon}^S \nabla\varphi \,\mathrm{d}\Omega\\
L_t(\mathbf{t}, \mathbf{v}) &= \int_{\Gamma_{\mathbf{t}}} \mathbf{t} \cdot \mathbf{v} \,\mathrm{d}\Gamma\\
L_d(d, \varphi) &= \int_{\Gamma_d} d\varphi \,\mathrm{d}\Gamma
\end{aligned}
\tag{14}
$$

and

$$
\begin{aligned}
V_a &= \{\mathbf{v} = v_i \bar{\mathbf{e}}_i, \varphi \text{ with } \mathbf{v} = 0 \text{ on } \Gamma_u \text{ and}\\
&\quad \nabla\varphi = \nabla\varphi_S \text{ in } S, i = 1 \text{ or } 3\}\\
V_b &= \{\mathbf{v} = v_i \bar{\mathbf{e}}_i, \varphi \text{ with } \mathbf{v} = 0 \text{ on } \Gamma_u, i = 1 \text{ or } 3\}\\
V_c &= \{\mathbf{v} = v_i \bar{\mathbf{e}}_i, \varphi \text{ with } \mathbf{v} = 0 \text{ on } \Gamma_u, \text{ and}\\
&\quad \nabla\varphi = 0 \text{ in } S, i = 1 \text{ or } 3\}.
\end{aligned}
$$

Here S denotes the design domain, Θ denotes the volume of piezoceramic type 1 material in the design domain, and Θ_1 denotes the upper-bound volume constraint defined to limit the maximum amount of material type 1. The other constraints are equilibrium equations for the piezoelectric medium (see section 2) considering different load cases. These equations are solved separately from the optimization problem. They are stated in the problem to indicate that, whatever topology is obtained, it must satisfy the equilibrium equations. The present notation follows closely the one by Bendsøe and Kikuchi (1988).

4. Numerical implementation

The continuum distribution of design variable $\rho_1(\mathbf{x})$ is given by the function (Matsui and Terada 2004, Rahmatalla and Swan 2004):

$$
\rho_1(\mathbf{x}) = \sum_{I=1}^{n_d} \rho_{1\mathrm{I}} N_I(\mathbf{x}) \tag{15}
$$

where $\rho_{1\mathrm{I}}$ is a nodal design variable, N_I is the finite element shape function that must be selected to provide non-negative values of the design variables, and n_d is the number of nodes at each finite element. The design variable $\rho_{1\mathrm{I}}$ can assume different values at each node of the finite element. The additional design variable $\rho_2(\mathbf{x})$ is assumed to be uniform inside each finite element, and, in the discretized form, becomes the design variable $\rho_{2\mathrm{e}}$.

Due to the definition of equation (15), the material property functions (equations (8) and (9)) also have a continuum distribution inside the design domain. Thus, considering the mathematical definitions of the stiffness and piezoelectric matrices of equation (3), the material properties must remain inside the integrals and be integrated together by means of the graded finite element concept (Kim and Paulino 2002).

By means of the FE matrix formulation of equilibrium (see equation (3)), the mean transduction (see equation (10)) and the mean compliance (see equation (11)) can be calculated numerically using the following expressions (Silva *et al* 2000):

$$
\begin{aligned}
L_2(\mathbf{U}_1, \boldsymbol{\Phi}_1) &= \{\mathbf{U}_1\}^{\mathrm{t}}\{\mathbf{F}_2\} + \{\boldsymbol{\Phi}_1\}^{\mathrm{t}}\{\mathbf{Q}_2\} = \{\mathbf{U}_1\}^{\mathrm{t}}\{\mathbf{F}_2\}\\
&= \{\mathbf{U}_1\}^{\mathrm{t}}[\mathbf{K}_{u\phi}]\{\boldsymbol{\Phi}_2\} - \{\boldsymbol{\Phi}_1\}^{\mathrm{t}}[\mathbf{K}_{\phi\phi}]\{\boldsymbol{\Phi}_2\} \qquad (16)\\
L_3(\mathbf{U}_3, \boldsymbol{\Phi}_3) &= \{\mathbf{U}_3\}^{\mathrm{t}}\{\mathbf{F}_3\} + \{\boldsymbol{\Phi}_3\}^{\mathrm{t}}\{\mathbf{Q}_3\} = \{\mathbf{U}_3\}^{\mathrm{t}}\{\mathbf{F}_3\}\\
&= \{\mathbf{U}_3\}^{\mathrm{t}}[\mathbf{K}_{uu}]\{\mathbf{U}_3\} + \{\mathbf{U}_3\}^{\mathrm{t}}[\mathbf{K}^{\mathrm{t}}_{u\phi}]\{\boldsymbol{\Phi}_3\}. \qquad (17)
\end{aligned}
$$

Notice that $\{\boldsymbol{\Phi}_1\}^{\mathrm{t}}\{\mathbf{Q}_2\} = 0$ (because $\{\mathbf{Q}_2\} = 0$) and $\{\boldsymbol{\Phi}_3\}^{\mathrm{t}}\{\mathbf{Q}_3\} = 0$ (because $\{\boldsymbol{\Phi}_3\} = 0$). The expression for $L_4(\mathbf{U}_1, \boldsymbol{\Phi}_1)$ is equal to equation (16) by substituting $\{\mathbf{F}_2\}$ by $\{\mathbf{F}_4\}$ and $\{\mathbf{Q}_2\}$ by $\{\mathbf{Q}_4\}$. The finite element equilibrium, equation (3), is solved considering four-node isoparametric finite elements under plane-strain assumptions.

A relevant problem to be solved is how to define the piezoceramic electrodes. In previous design optimization problems for piezoelectric actuators (Silva *et al* 2000, Carbonari *et al* 2005), the piezoceramic domain remains fixed and only the coupling structural domain (elastic material) is changed. Thus, the position of electrodes is known. However, if non-piezoelectric (such as gold) and piezoelectric material are distributed in the design domain the position of the piezoceramic electrodes cannot be defined '*a priori*' because the piezoceramic location is not known in the design domain. To circumvent this problem, we consider the electrical problem independently for each finite element by defining a pair of electrodes at each finite element. Thus, each finite element has its own electrical degrees of freedom, as illustrated by figure 3, in which u_i and v_i denote the node i horizontal and vertical displacements, respectively, and ϕ_{ij} denotes the jth potential at the ith node (Carbonari *et al* 2007).

As illustrated by figure 3, each finite element has four electrical degrees of freedom given by $[\phi_a, \phi_b, \phi_c, \phi_d]$ (nodes are ordered counterclockwise starting from the upper right corner of each finite element) considering that one of the

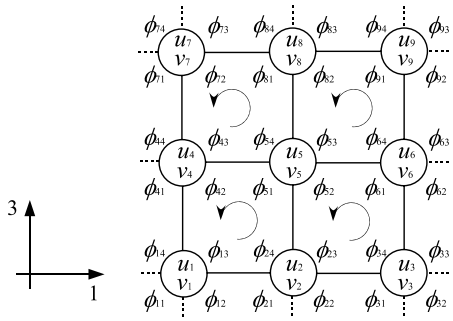

Figure 3. Finite elements with their corresponding electrical degrees of freedom. Here, u_i and v_i denote the node i horizontal and vertical displacement, respectively, and ϕ_{ij} denotes the jth potential at the ith node.

electrodes is grounded. Electrical voltage ϕ_0 is applied to the two upper nodes, and thus, the four electrical degrees of freedom are specified at each finite element as follows ($[\phi_0, \phi_0, 0, 0]$). This is equivalent to applying a constant electrical field along the 3-direction in the design domain (see figure 3).

The discretized form of the final optimization problem is stated as

$$\begin{aligned}
&\text{Maximize: } \mathcal{F}(\rho_{1I}, \rho_{2e}) \\
&\rho_{1I}, \rho_{2e} \\
&\text{subject to } \{\mathbf{F}_3\} = -\{\mathbf{F}_2\} \quad (\Gamma_{\mathbf{t}_3} = \Gamma_{\mathbf{t}_2}) \\
&\qquad \{\mathbf{F}_4\}^{\mathrm{t}}\{\mathbf{F}_2\} = 0 \quad (\Gamma_{\mathbf{t}_4} = \Gamma_{\mathbf{t}_2}) \\
&\qquad [\mathcal{K}_1]\{\mathcal{U}_1\} = \{\mathcal{Q}_1\} \qquad [\mathcal{K}_2]\{\mathcal{U}_2\} = \{\mathcal{Q}_2\} \\
&\qquad [\mathcal{K}_3]\{\mathcal{U}_3\} = \{\mathcal{Q}_3\} \qquad [\mathcal{K}_2]\{\mathcal{U}_4\} = \{\mathcal{Q}_4\} \\
&\qquad 0 \leqslant \rho_{1I} \leqslant 1 \qquad I = 1 \ldots N_{\mathrm{des}} \\
&\qquad 0 \leqslant \rho_{2e} \leqslant 1 \qquad e = 1 \ldots \mathrm{NEL} \\
&\qquad \textstyle\sum_{i=1}^{N_{\mathrm{des}}} \rho_{1I} V_I - \Theta_1 \leqslant 0
\end{aligned} \tag{18}$$

where V_I denotes the volume associated with each finite element node, which is equal to the finite element volume. The parameter N_{des} denotes the number of nodes in the design domain, which is equal to the number of design variables in this work, and NEL is the number of elements in the piezoceramic design domain. The matrices $[\mathcal{K}_1]$ and $[\mathcal{K}_3]$ are reduced forms of the matrix $[\mathcal{K}_2]$ considering non-zero and zero prescribed voltage degrees of freedom in the domain, respectively. The initial domain is discretized by finite elements and the design variables are the values of $\rho_{1\mathrm{I}}$ and $\rho_{2\mathrm{e}}$ defined at each node or at each finite element, respectively. The boundary conditions for the piezoceramic domain for load cases (a1), (a2), (b), and (c) of figure 2 are shown in figure 4.

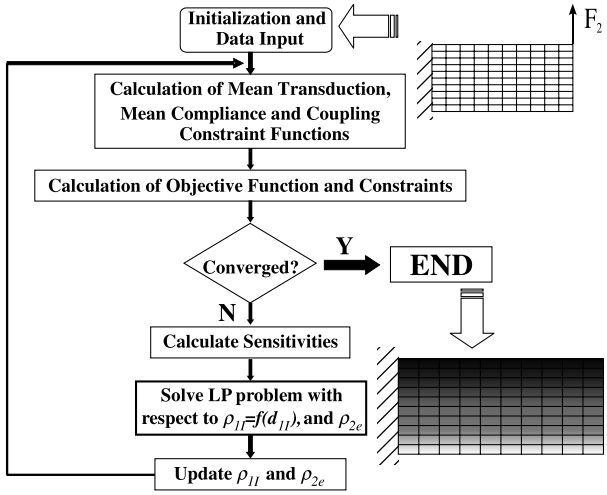

Figure 5. Flow chart of optimization procedure (LP means linear programming).

A flow chart of the optimization algorithm describing the steps involved is shown in figure 5. The software was implemented using the C language. Mathematical programming using Sequential Linear Programming (SLP) is applied to solve the optimization problem, which is appropriate when there are a large number of design variables, and different objective functions and constraints (Vanderplaatz

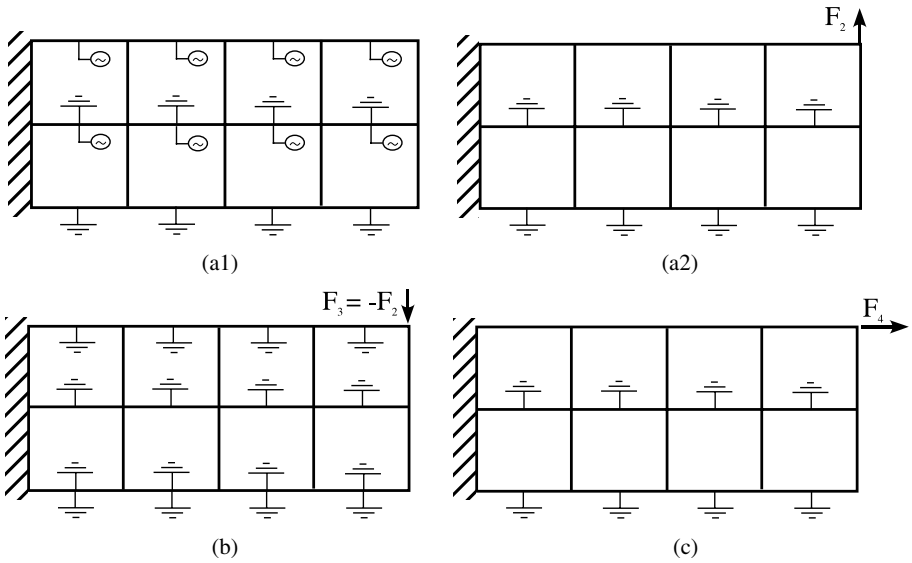

Figure 4. General electrical boundary conditions for the design domain: (a1) and (a2) mean transduction; (b) mean compliance; (c) coupling constraint function.

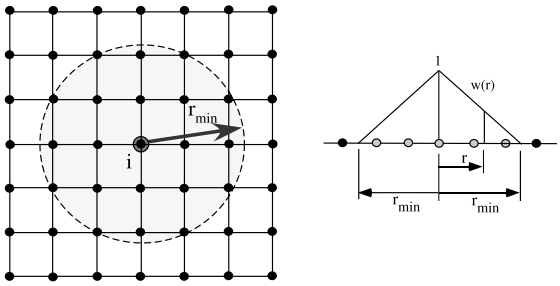

Figure 6. Projection technique adapted to the CAMD concept. Notice that the projection cone is centered at a nodal point.

1984, Hanson and Hiebert 1981). The linearization of the problem at each iteration requires the sensitivities (gradients) of the multi-objective function and constraints. These sensitivities depend on gradients of mean transduction and mean compliance functions in relation to ρ_{1I} and ρ_{2e} (derived in appendix A).

Suitable moving limits are introduced to assure that the design variables do not change by more than 5–15% between consecutive iterations. A new set of design variables ρ_{1I} and ρ_{2e} is obtained after each iteration, and the optimization continues until convergence is achieved for the objective function. The value of the penalization coefficient p_e is set equal to 1 (Kögl and Silva 2005) (see equation (9)).

5. Projection of material distribution

The CAMD approach ensures a continuous material distribution across elements. However, it does not provide a general control of the gradient of material distribution. Topology optimization filters available in the literature (Bendsøe and Sigmund 2003) to control material distribution allow only an implicit control of the material gradation. Thus, in this work, we introduce a new layer of design variables and apply projection functions (Guest *et al* 2004) on top of the CAMD to have an explicit control of the material gradation. This projection technique is applied only to design variable ρ_1, which is associated to the control of material gradation.

Let y_n denote all design variables associated with nodes, and ρ_{1n} the values of material density at the nodes. Assume that the required change of material density must occur over a minimum length scale $r_{\min}$. By means of the projection function (f), ρ_{1n} can be obtained from y_n as follows (assuming that four-node element is used):

$$\rho_{1n} = f(y_n), \tag{19}$$

where f is the projection function defined as follows:

$$\rho_{1i} = f(y_j) = \frac{\sum_{j\in S_i} y_j\, W\, r_{ij}}{\sum_{j\in S_i} W\, r_{ij}}, \tag{20}$$

where r_{ij} is the distance between nodes j and i:

$$r_{ij} = \|\mathbf{x}_j - \mathbf{x}_i\|, \tag{21}$$

and S_i is the set of nodes in the domain under the influence of node i, which consists of a circle of radius $r_{\min}$ with center at node i. The weight function W (see equation (20)) is defined as follows:

$$W(r_{ij}) = \begin{cases} \dfrac{r_{\min} - r_{ij}}{r_{\min}} & \text{if } \mathbf{x}_j \in S_i \\ 0 & \text{otherwise.} \end{cases} \tag{22}$$

Figure 6 illustrates the idea of the projection technique. As a consequence, the topology optimization problem definition must be revised accordingly.

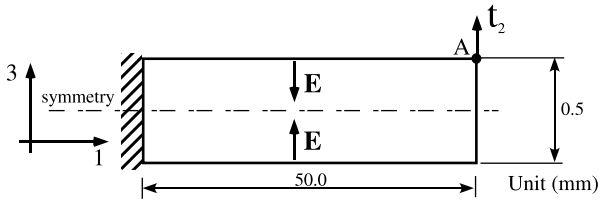

Figure 7. Bimorph design domain.

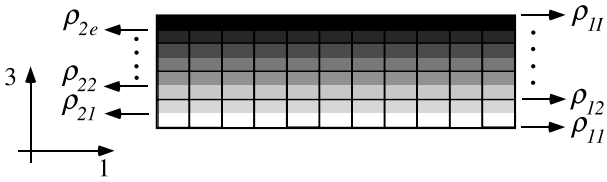

Figure 8. Bimorph design domain divided into horizontal layers. Design variables ρ_{1I} and ρ_{2e} are defined for each interfacial layer and each layer, respectively.

6. FGM bimorph-type piezoactuators

The design of FGM bimorph-type piezoactuators is presented to illustrate the proposed method. A bimorph actuator is made of plates (or shells) composed by at least two layers of piezoelectric material, usually with opposite polarization. It may also contain layers of non-piezoelectric materials. An FGM bimorph has graded piezoceramics in the lower and upper layers. Here we use the name bimorph associated with the fact that we have two domains with opposite polarization.

The idea is to simultaneously distribute two types of piezoelectric material or a non-piezoelectric (in this case, gold) and a piezoelectric material. The design domain (for all results) is shown in figure 7. The adopted discretization consists of 10 500 finite elements (a rectangle discretized by a 500 × 21 mesh). The bimorph is essentially a piezoelectric cantilever-type actuator. The design domain is divided into 21 horizontal layers and design variables ρ_{1I} and ρ_{2e} are considered for each interfacial layer and each layer, respectively, as described in figure 8. Thus, there are 22 design variables ρ_{1I} and 21 design variables ρ_{2e}. The mechanical and electrical boundary conditions are shown in figure 7. Notice that the electrical field is applied to the entire design domain; however, the location of the actual piezoceramic region is not known '*a priori*'. Figure 9 illustrates three possible situations that may occur during the optimization regarding the distribution of piezoceramic material (middle, outer or inner layers) in the symmetric part of design domain. In this case, the gold region will not be influenced by the electric field because the piezoelectric effect is null (see equation (6)).

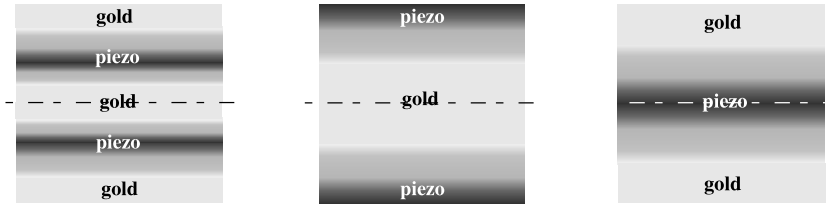

(a) (b) (c)

Figure 9. Possible situations that may occur in the symmetric part of the design domain during the optimization: (a) piezoceramic region in the middle layers; (b) piezoceramic region in the outer layers; (c) piezoceramic regions in the inner layers.

Table 1. Material properties of piezoceramic PZT5A (Ikeda 1996).

c_{11}^E (10^{10} N m^{-2})	12.1	e_{13} (C m^{-2})	−5.4
c_{12}^E (10^{10} N m^{-2})	7.54	e_{33} (C m^{-2})	15.8
c_{13}^E (10^{10} N m^{-2})	7.52	e_{15} (C m^{-2})	12.3
c_{33}^E (10^{10} N m^{-2})	11.1		
c_{44}^E (10^{10} N m^{-2})	2.30		
c_{66}^E (10^{10} N m^{-2})	2.10		

Table 1 presents the piezoelectric material properties used in the simulations (for all examples). The Young's modulus and Poisson's ratio of gold are equal to 83 GPa and 0.44, respectively (Brady *et al* 1997). Two-dimensional isoparametric finite elements under plane-strain assumption are used in the finite element analysis.

For all examples, unless otherwise specified, the electric field applied to the design domain is equal to 420 V mm^{-1} (see figure 7). The objective consists of maximizing the output displacement at point A (see figure 7). The displacement coupling constraint is not activated, and thus the coefficient β is equal to zero in all cases. The initial value for design variables (ρ_{1I}) is equal to 0.45 in all cases, and ρ_{2e} is equal to 0.1. Thus, the optimization problem starts in the feasible domain (all constraints satisfied). The projection technique is applied only for design variable ρ_{1I}. The results are shown by plotting the pseudo-density gradation variation along layers. Through material models described by equations (8) and (9), the property gradation variation and polarization sign can be obtained. For the examples of sections 6.1 and 6.2, the material type 1 is PZT5A (see properties in table 1) and the material type 2 is gold.

6.1. *Influence of property gradation*

In the first set of results, only property gradation (associated with design variable ρ_{1I}) is considered. Thus, the design variables ρ_{2e} are kept fixed and equal to 0.0 and 1.0 for the half upper and half lower layers, respectively. A symmetry constraint is imposed in the middle horizontal axis for the pseudo-density distribution, otherwise an exactly symmetric distribution cannot be guaranteed due to the influence of small differences of sensitivity values in the final optimization result. The topology optimization results obtained considering the value of the weight coefficient w (see equation (12)) equal to 0.2 or 1.0, and Θ_1 equal to 50% or 100%, are shown in figure 10. The value of $r_{\min}$ is set equal to 0.025 mm, 0.1 mm, 0.125 mm, and 0.15 mm for these results. By setting the value of $r_{\min}$ equal to 0.025 mm, which is equal to the element length, the projection technique is deactivated in the design problem. The optimization finished with the constraint Θ_1 active for all designs. For the case illustrated by figure 10(c), the associated convergence curves of objective function, mean compliance, and mean transduction are shown in figure11. The convergence curves for the other results of figure 10 are similar.

Table 2. Displacements at point A (420 V mm^{-1} applied).

Bimorph (piezo/Au)	u_z (mm)	w	Θ_1%	$r_{\min}$ (mm)
Figure 10(a)	0.338	0.2	50	0.025[a]
	0.341	0.2	50	0.1
	0.343	0.2	50	0.125
	0.343	0.2	50	0.15
Figure 10(b)	0.404	0.2	100	0.025[a]
	0.419	0.2	100	0.1
	0.430	0.2	100	0.125
	0.432	0.2	100	0.15
Figure 10(c)	0.483	1.0	50	0.025[a]
	0.466	1.0	50	0.1
	0.454	1.0	50	0.125
	0.439	1.0	50	0.15
Figure 10(d)	0.711	1.0	100	0.025[a]–0.15
Figure 12	0.341	0.2	50	0.025[a]
	0.346	0.2	50	0.1

[a] Projection deactivated.

Table 2 describes vertical displacement (u_z) at point A (see figure 7) considering 420 V mm^{-1} applied to the piezoceramic domain for the bimorph designs. The X displacement is not presented because it is almost zero due to the weak coupling between horizontal (X) and vertical (Z) displacements.

From table 2, low values of w (0.2) correspond to a stiff design, and the largest displacements are obtained for w equal to 1.0 (see figure10(c)), as expected. For w equal to 0.2 and Θ_1 equal to 50%, the method provides an interesting graded solution with the lowest u_z displacement. By increasing the piezoceramic volume constraint (Θ_1 equal to 100%) the method does not use all the piezoceramic, and allocates some gold in the upper and lower layers. For w equal to 1 and Θ_1 equal to 50%, we note that the method tries to keep the piezoceramic material in the upper and lower layers and gold in the center. This material distribution will depend on the stiffness ratio between the piezoceramic and gold. The projection technique ($r_{\min} > 0.025$ mm) leads to a smooth material gradation; however, for the result from figure 10(a) regions with pure piezoceramic or pure gold are not obtained. In addition, the projection technique seems to contribute to

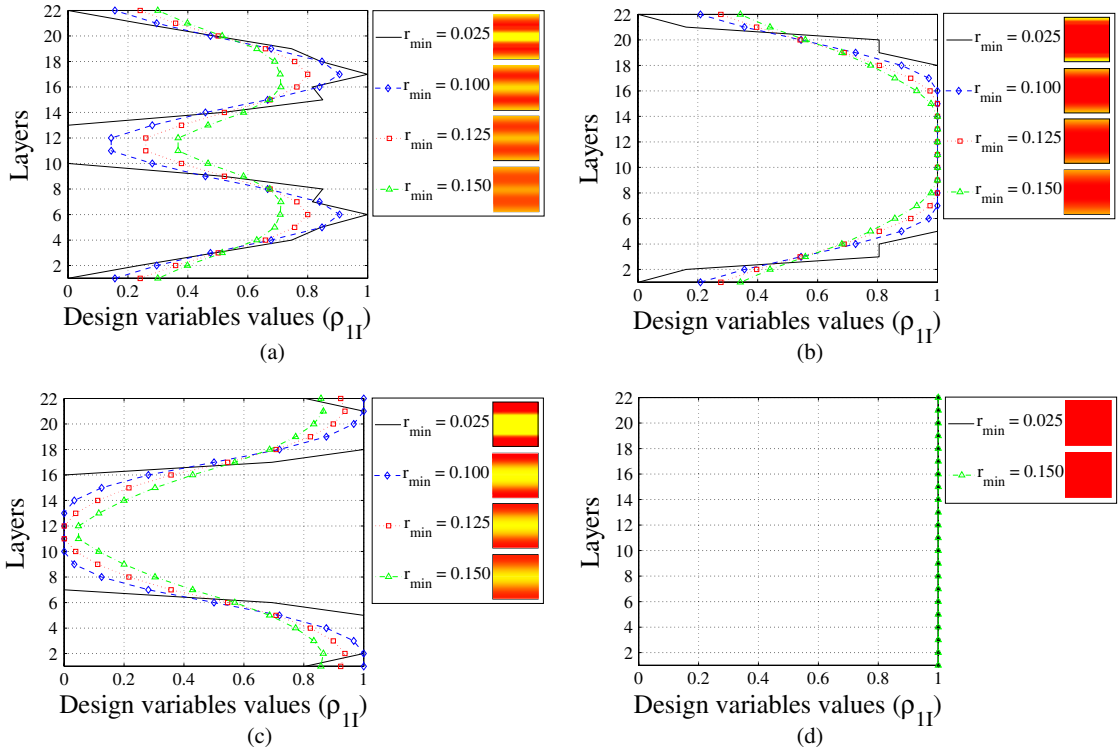

Figure 10. Optimal ρ_1 values along layer numbers obtained by distributing piezoelectric and gold materials in the domain. A symmetry constraint is imposed only for the cases without projection, i.e. $r_{\min} = 0.025$ mm (which is equal to the element length): (a) $w = 0.2$ and $\Theta_1 = 50\%$; (b) $w = 0.2$ and $\Theta_1 = 100\%$; (c) $w = 1.0$ and $\Theta_1 = 50\%$; (d) $w = 1.0$ and $\Theta_1 = 100\%$.

smooth the convergence curve, as shown in figure 11(b). The increase of the gradation length scale ($r_{\min}$) contributes to increase the output displacement for results from figures 10(a) and (b), and to decrease it for the result from figure 10(c). For w equal to 1 and Θ_1 equal to 100% (see figure 10(d)), we obtain homogeneous piezoceramic as the solution, and the largest output displacement (see table 2).

When the projection technique is not used, the optimization algorithm tends to obtain a material gradation with high property gradients, almost close to a 0–1 design, even though no penalization is applied. These sharp material gradations are difficult to manufacture. Thus, the implementation of a property gradient control is important for FGM manufacturing purposes.

6.2. *Influence of property gradation and polarization sign*

For the next set of results, both the property gradation variation (ρ_{1I}) and polarization sign change (ρ_{2e}) are considered. No symmetry constraint is imposed as the idea in this example is not to limit the optimality range of the result, but to seek an upper bound for the output displacement. The topology optimization results are obtained considering the same values of w, Θ_1, and $r_{\min}$ parameters as in the previous example; however, only the results for $w = 0.2$ and Θ_1 equal to 50% are shown in figure 12. Because the convergence curves are similar to the previous results, they are not shown.

For all the results, a change in the polarization sign is obtained from lower to upper layers (see for example, figure 12), recovering the usual pattern of bimorph achieved previously (see figure 10) showing that the change of polarization sign is not as significant as material gradation. A material gradation pattern similar to the previous results (see figure 10) is obtained for all results. We notice that, by using the projection technique ($r_{\min} > 0.025$ mm), a symmetric result is obtained, even though a symmetry constraint is not explicitly imposed. This does not happen when the projection technique is deactivated ($r_{\min} = 0.025$ mm). These results also show that a symmetric property gradation seems to be the optimum solution.

6.3. *Influence of property gradation considering piezoelectric materials only*

For the next examples, the material type 1 is piezoelectric material (see properties in table 1) and the material type 2 is also a piezoelectric material whose property values are given by Almajid *et al* (2001):

$$\begin{aligned} \mathbf{C}_1 &= 4.375 * \mathbf{C}_{\text{Tab1}}; \qquad & \mathbf{e}_1 &= 2.5 * \mathbf{e}_{\text{Tab1}}; \\ \mathbf{C}_2 &= 0.1 * \mathbf{C}_{\text{Tab1}}; \qquad & \mathbf{e}_2 &= 0.6 * \mathbf{e}_{\text{Tab1}}. \end{aligned} \tag{23}$$

Similarly to the previous example (see section 6.1), initially only the property gradation is considered; that is, only design variable ρ_{1I}. Thus, the design variables ρ_{2e} are kept fixed and equal to 0.0 and 1.0 for the half upper and half lower layers, respectively. A symmetry constraint is imposed in the middle horizontal axis for the pseudo-density distribution. The topology optimization results obtained considering the value of w coefficient (see equation (12)) equal to 0.5 or 1.0, and Θ_1 equal to 50% or 100%, respectively, are shown in figure 13. The value of $r_{\min}$ is set equal to 0.025 mm and 0.1 mm for these

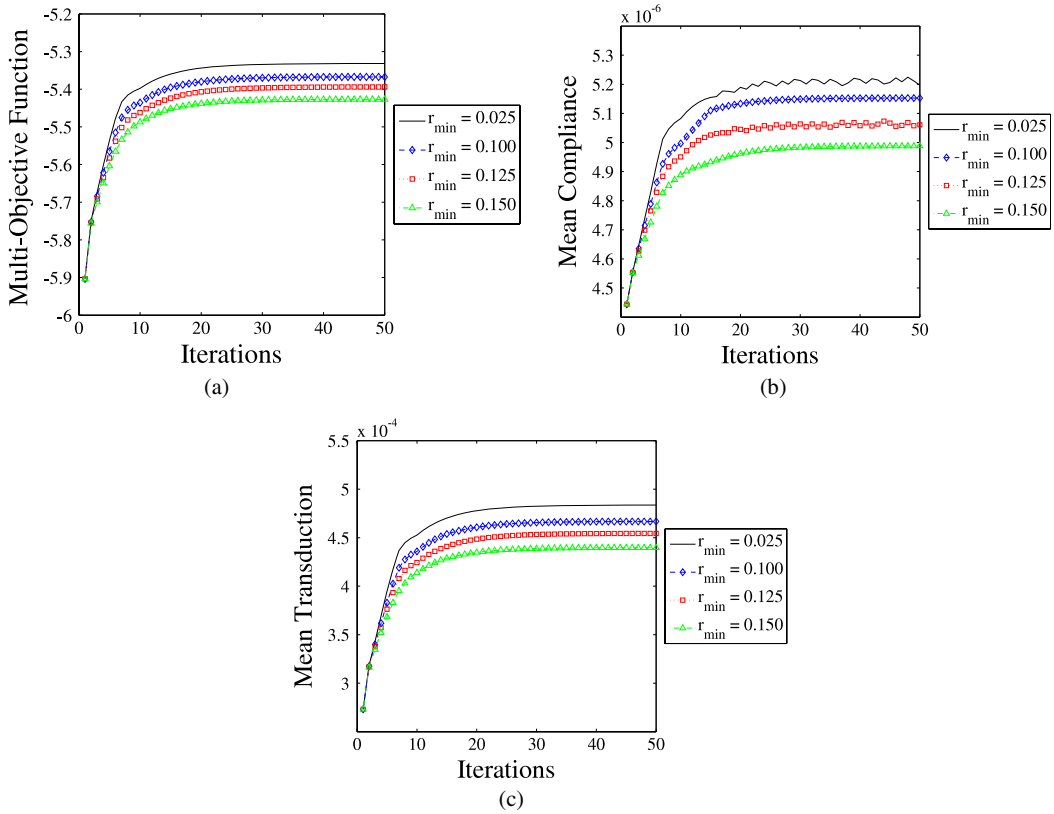

Figure 11. Convergence curves associated to figure 10(c) ($w = 1.0$ and $\Theta_1 = 50\%$): (a) objective function; (b) mean compliance; (c) mean transduction.

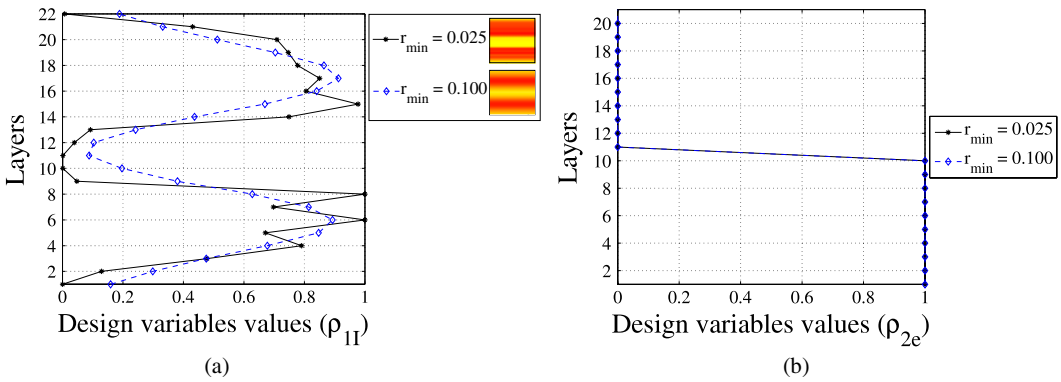

Figure 12. Optimal ρ_1 and ρ_2 values along layer numbers obtained by distributing piezoelectric and gold materials in the piezoceramic domain: $w = 0.2$ and $\Theta_1 = 50\%$. No symmetry constraint is imposed and projection is applied to ρ_1 only: (a) ρ_1 values; (b) ρ_2 values.

results. The results for w equal to 1.0, and Θ_1 equal to 50% or 100% are identical. Table 3 gives the vertical displacement (u_z) at point A (see figure 7) considering 420 V mm^{-1} applied to the piezoceramic domain for the resulting bimorph designs. The X displacement is not presented as it is almost zero, as explained before. For the case illustrated by figure 13(a), the associated convergence curves of objective function, mean compliance, and mean transduction are shown in figures 14(a)–(c), respectively. The convergence curves for the other results of figure 13 are similar.

For w equal to 0.5 and Θ_1 equal to 50% (figure 13 (a)), the optimization algorithm places piezoceramic material type 1 (stiff material) in the upper and lower layers, and piezoceramic material type 2 (soft material) in the center layers of the design domain. Again, the projection technique ($r_{\min} > 0.025$ mm) leads to a smooth material gradation profile.

However, when considering Θ_1 equal to 100% a homogeneous material made of only piezoceramic type 1 is obtained (see figure 13(b)). This happens because w equal to 0.5 implies stiffer designs (see displacements in table 3), and piezoceramic material type 1 is stiffer than piezoceramic material type 2. For results considering w equal to 1.0, a homogeneous material is also obtained, however, made only of piezoceramic type 2. The parameter w equal to 1.0 implies

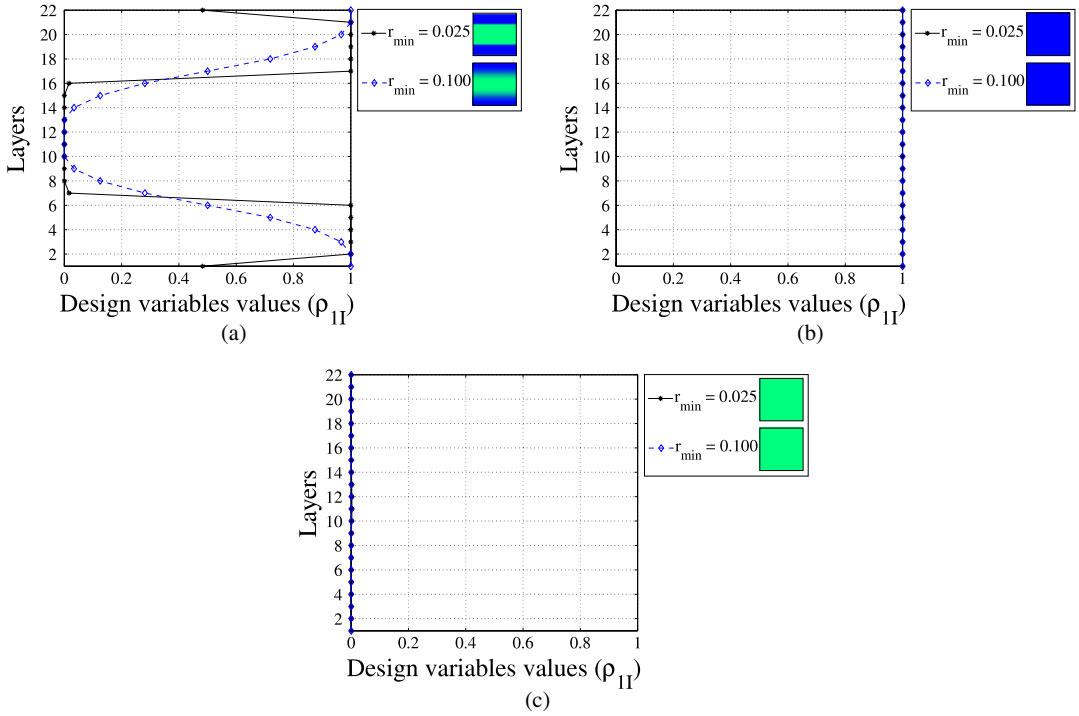

Figure 13. Optimal ρ_1 values along layer numbers obtained by distributing piezoelectric materials type 1 and 2 in the piezoceramic domain. A symmetry constraint is imposed: (a) $w = 0.5$ and $\Theta_1 = 50\%$; (b) $w = 0.5$ and $\Theta_1 = 100\%$; (c) $w = 1.0$ and $\Theta_1 = 50\%$ or 100%.

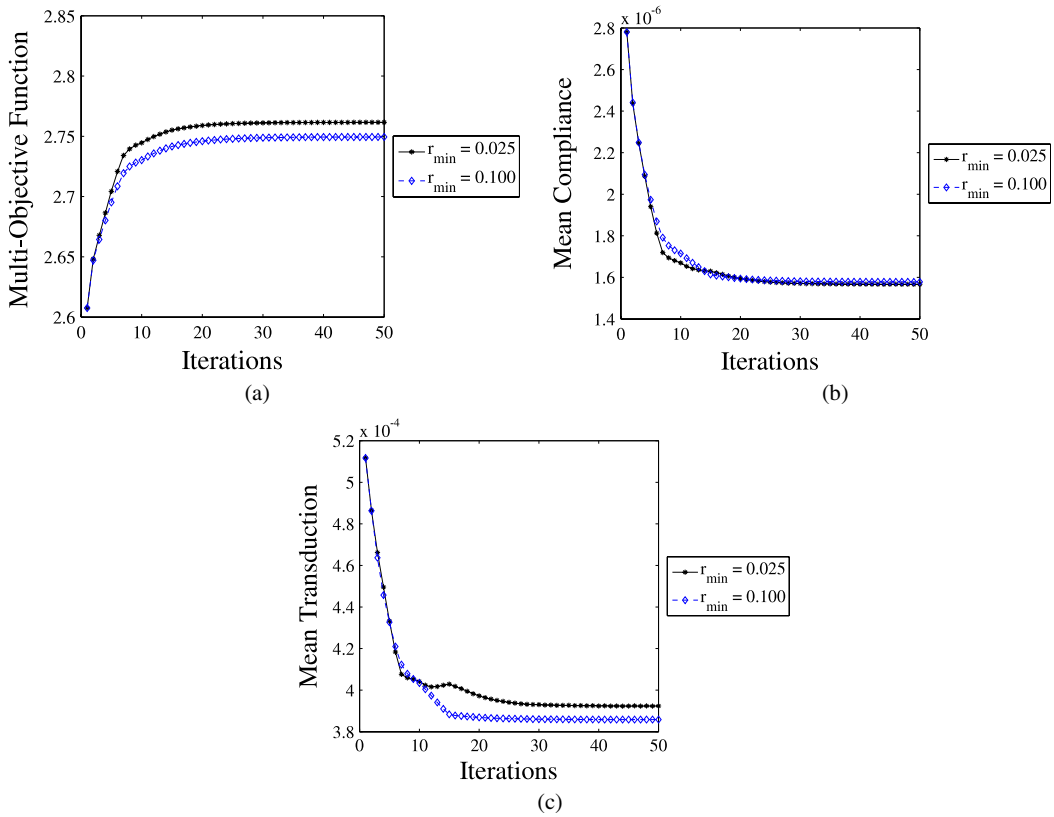

Figure 14. Convergence curves associated to figure 13 (a) considering piezoelectric materials type 1 and type 2 ($w = 0.5$ and $\Theta_1 = 50\%$): (a) objective function; (b) mean compliance; (c) mean transduction.

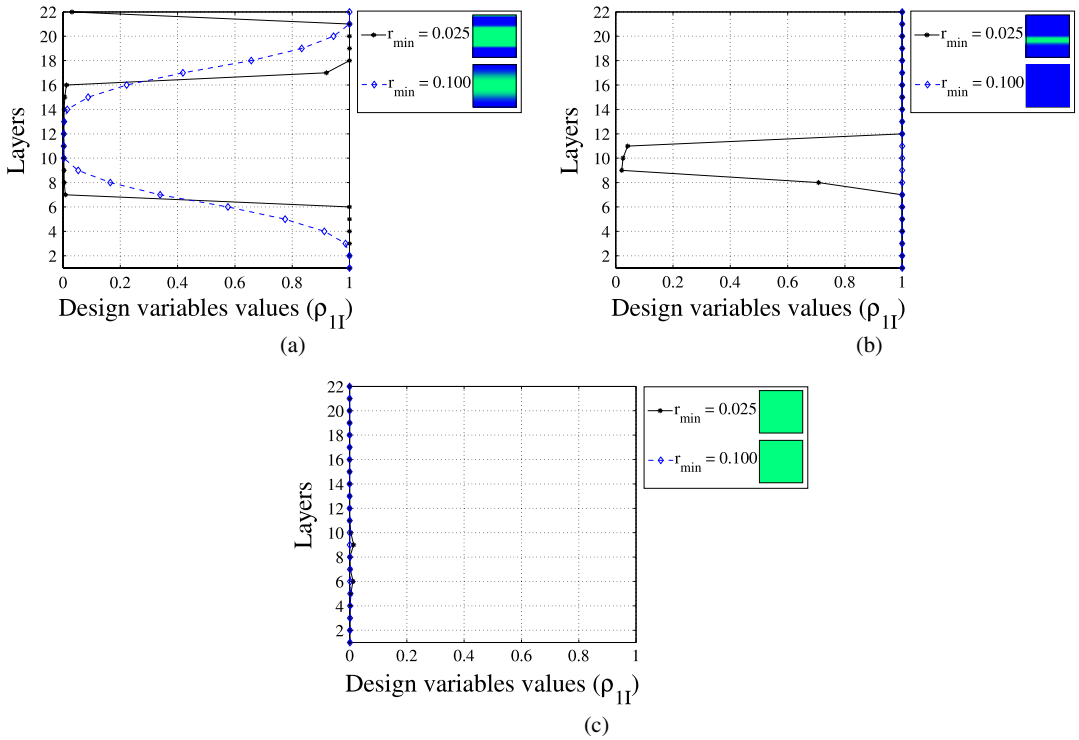

Figure 15. Optimal ρ_1 values along layer numbers obtained by distributing piezoelectric materials type 1 and 2 in the piezoceramic domain. No symmetry constraint is imposed: (a) $w = 0.5$ and $\Theta_1 = 50\%$; (b) $w = 0.5$ and $\Theta_1 = 100\%$; (c) $w = 1.0$ and $\Theta_1 = 50\%$ or 100%.

Table 3. Displacements at point A (420 V mm^{-1} applied).

Bimorph (Piezo/Au)	u_z (mm)	w	Θ_1%	$r_{\min}$ (mm)
Figure 13(a)	0.392	0.5	50	0.025[a]
	0.385	0.5	50	0.1
Figure 13(b)	0.407	0.5	100	0.025[a] or 0.1
Figure 13(c)	4.19	1.0	50 or 100	0.025[a] or 0.1
Figure 15(a)	0.389	0.5	50	0.025[a]
	0.382	0.5	50	0.1
Figure 15(b)	0.385	0.5	100	0.025[a]
	0.388	0.5	100	0.1
Figure 15(c)	3.57	1.0	50 or 100	0.025[a]
	3.76	1.0	50 or 100	0.1

[a] Projection deactivated.

more flexible designs (see displacement in table 3). Thus, in this case, the optimization chooses piezoceramic material type 2, and 10 times larger displacement is obtained. Recall that the volume constraint is defined for material type 1 only.

6.4. Influence of property gradation and polarization sign considering piezoelectric materials only

For the next set of results, the property gradation variation (ρ_{1I}) and polarization sign change (ρ_{2e}) are considered. No symmetry constraint is imposed because the idea again is not to limit the optimality range of the result, but to seek an upper bound for the output displacement. The topology optimization results are obtained considering the value of the weight coefficient w (see equation (12)) equal to 0.5 or 1.0, Θ_1 equal to 50% or 100%, and $r_{\min}$ equal to 0.025 mm (projection deactivated) and 0.1 mm, as illustrated in figures 15 and 16. Again, the results for w equal to 1.0, and Θ_1 equal to 50% or 100% are identical. Table 3 gives the vertical displacement (u_z) at point A (see figure 7) for the bimorph designs. The convergence curves are similar to the previous results; thus, they are not shown.

For all the results obtained, a change in the polarization sign is obtained from lower to upper layers recovering the usual pattern defined in the previous results (figure 13); however, the change of polarization sign is slightly shifted from the middle line (figure 16). This may be due to the fact that the projection technique is not considered for design variable ρ_{2e}. This also shows that change of polarization sign does not play a significant role in this problem. For w equal to 0.5, Θ_1 equal to 50%, and $r_{\min}$ equal to 0.1 mm (figure 15(a)), a symmetric material gradation pattern equal to the previous result of figure 13(a) is obtained; that is, the optimization algorithm places the symmetrically piezoceramic material type 1 in the upper and lower layers of the design domain. When the projection technique is not active ($r_{\min} = 0.025$ mm), the material gradation is slightly asymmetric (see figure 15(a)) and the displacement value is larger, as in the previous example. By increasing the volume constraint (Θ_1 equal to 100%), the result without the projection technique suggests a material variation; however, when the projection technique is applied, a homogeneous piezoceramic material type 1 is obtained (see figure 15(b)) like in the previous example (see figure 13(b)). As expected, these are stiffer designs (see displacements in table 3).

For w equal to 1.0 a homogeneous material is obtained (no material gradation) for soft material (type 2), generating a displacement 10 times larger than displacement for results considering w equal to 0.5 (see figures 15(a) and (b)).

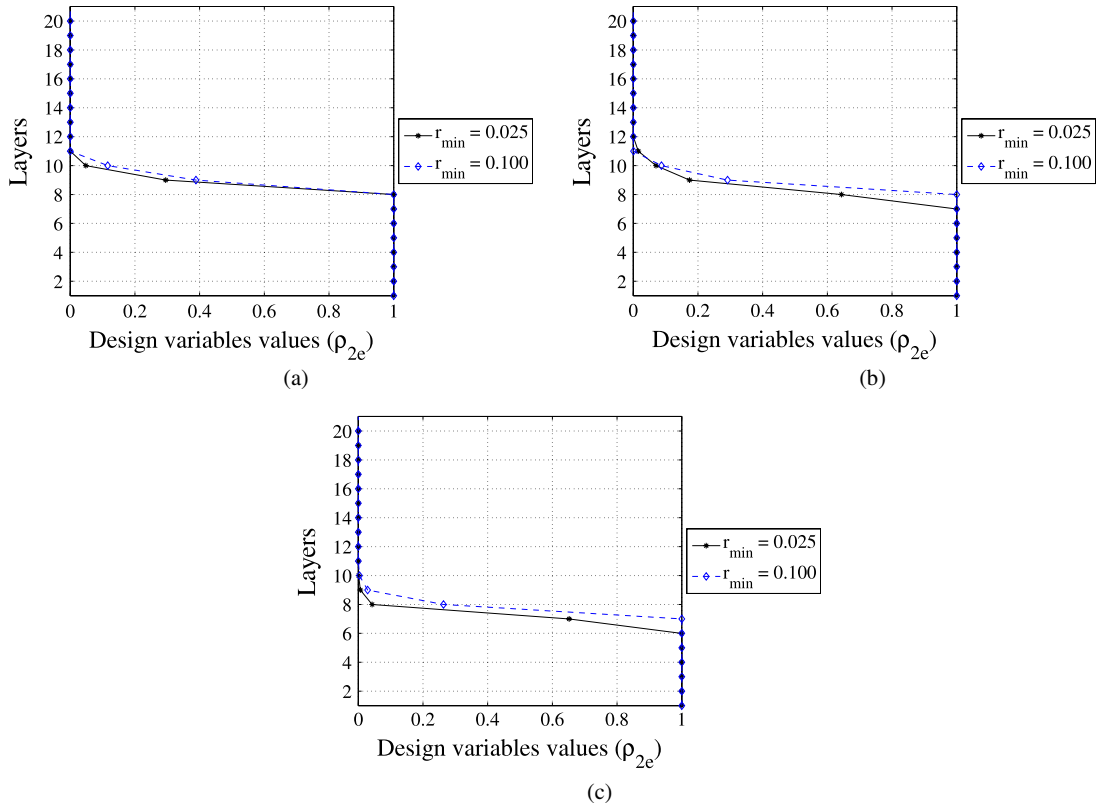

Figure 16. Optimal ρ_2 values along layer numbers obtained by distributing piezoelectric materials type 1 and 2 in the piezoceramic domain. No symmetry constraint is imposed: (a) $w = 0.5$ and $\Theta_1 = 50\%$; (b) $w = 0.5$ and $\Theta_1 = 100\%$; (c) $w = 1.0$ and $\Theta_1 = 50\%$ or 100%. Although r_{min} values are provided, projection is applied to ρ_1 only (and not ρ_2).

Comparing the results from figures 13(b) (with symmetry constraint) and 15(b) (without symmetry constraint), one notices that both generate output displacements of the same order; however, the one from figure 15(b) is smaller than the one from figure 13(b). Moreover, in the case of figure 15, a symmetric polarization sign distribution is not obtained, suggesting that the optimization method got trapped in a local minimum. The results from figures 13(c) and 15(c) are both homogeneous and generate the largest displacement values. The small difference of displacement values is due (again) to the fact that the change of polarization sign is slightly shifted from the middle line in figure 16(c) (also see figure 7) because the projection technique is not applied for design variable ρ_{2e}.

Thus, in this example, where two types of piezoelectric material are distributed, it seems that the material gradation does not play an important role as it occurs when piezoelectric material and gold are distributed. The inclusion of the polarization sign change (ρ_{2e}) in this and previous examples seems to guide the optimization to local minima solutions that have worse performance than when only material gradation is considered in the optimization. The projection technique helps to avoid local minima results, such as asymmetric results.

7. Conclusions

Topology optimization designs of FGM bimorph actuators are investigated with special emphasis on material gradation and polarization sign change in actuator performance. The topology optimization formulation allows the search for an optimal gradation of piezoelectric material properties and polarization sign in the design of FGM piezoelectric actuators to enhance their performance in terms of output displacement. The optimization problem allows the simultaneous distribution of either two piezoelectric materials or a non-piezoelectric (such as gold) and a piezoelectric material in the design domain, as well as the polarization sign. The adopted material model is based on the density method and it interpolates fictitious densities at each finite element. The interpolation is based on pseudo-densities defined as design variables for each finite element node, which provides a continuum material distribution in the domain. A projection technique is implemented that allows explicit control of the material gradation, which is very important when designing FGM piezoelectric actuators and structures.

For the specific examples considered, the material gradation plays an important role in increasing actuator performance when distributing piezoelectric and non-piezoelectric material (such as gold) in the design domain; however, the performance is not improved when distributing two types of piezoelectric material. In both cases, the inclusion of the polarization sign change as a design variable in the optimization problem does not play a significant role in the design problem, recovering the usual pattern of polarization defined for bimorph-type actuators, which corresponds to a change in the polarization sign from lower to upper layers. The projection technique helps to avoid local minima results, and asymmetric results. This fea-

ture is important for manufacturing purposes and can lead to substantially improved design.

As future work, other FGM piezoactuators can be optimized using the present approach, and different design criteria can be considered. For instance, in this work, the position of the electrodes is not defined in the domain when distributing piezoceramic and gold materials. To circumvent this problem, we have applied a constant electric field as electrical excitation to obtain the design. To this effect, we have constrained all electrical degrees of freedom and, as a consequence, the mechanical and electrical problems become decoupled. Thus, the dielectric properties do not influence the design, which is a limitation of the present approach. To address this problem, a potential alternative procedure consists of applying electrical voltage and allowing for movement of the electrode boundaries. In this case, the influence of the dielectric properties in the design problem are explicitly taken into account. Finally, computational simulation and design should be done in conjunction with manufacturing of the devices. The practical use of the present approach has the potential to broaden the range of application of functionally graded piezoelectric actuators in the field of smart structures.

Acknowledgments

The first author thanks CNPq (Conselho Nacional de Desenvolvimento Científico e Tecnológico—Brazil), for supporting him through a doctoral fellowship (No. 140687/2003-3). The second author thanks FAPESP (Fundação de Amparo à Pesquisa do Estado de São Paulo), CNPq, and the University of Illinois at Urbana-Champaign (UIUC) for inviting him as a visiting Professor at UIUC during the Summer/2006 and 2007. The third author thanks the University of São Paulo (USP) for inviting him as a Visiting Professor in 2006 and 2007. We gratefully acknowledge the USA NSF through the project CMS#0303492 (Inter-Americas Collaboration in Materials Research and Education, PI Professor W Soboyejo, Princeton University).

Appendix A. Sensitivity analysis using the adjoint method

The gradient of the function $\mathcal{F}$ relative to the design variable A_I (either $\rho_{1\mathrm{I}}$ or $\rho_{2\mathrm{e}}$) is obtained by differentiating equation (12), which results in a expression that depends on the sensitivities of mean transduction, mean compliance, and coupling constraint function. The sensitivity of the mean transduction considering electrical field excitation is obtained by differentiating equation (16) (Carbonari *et al* 2005):

$$\frac{\partial L_2(\mathbf{U}_1, \Phi_1)}{\partial A_I} = \{\mathbf{F}_2\}^{\mathrm{t}} \left\{ \frac{\partial \mathbf{U}_1}{\partial A_I} \right\}. \tag{A.1}$$

Notice that $\partial \mathbf{F}_2 / \partial A_I = 0$ as it does not depend on design variables because $\mathbf{F}_2$ is a unit dummy load. The sensitivity $\partial \mathbf{U}_1 / \partial A_I$ is obtained by differentiating equation (6), resulting in the following expression:

$$\begin{aligned} &[\mathbf{K}_{uu}]\{\mathbf{U}_1\} = \{\mathbf{F}_1\} - [\mathbf{K}_{u\phi}]\{\mathbf{\Phi}_1\} \\ &\quad \Rightarrow [\mathbf{K}_{uu}] \frac{\partial \{\mathbf{U}_1\}}{\partial A_I} = -\frac{\partial [\mathbf{K}_{u\phi}]}{\partial A_I}\{\mathbf{\Phi}_1\} - \frac{\partial [\mathbf{K}_{uu}]}{\partial A_I}\{\mathbf{U}_1\}. \end{aligned} \tag{A.2}$$

In addition, notice that $\partial \mathbf{F}_1 / \partial A_I = 0$ as it does not depend on design variables because $\mathbf{F}_1$ is an applied load. Moreover, $\partial \mathbf{\Phi}_1 / \partial A_I = 0$ because all electrical voltage degrees of freedom are prescribed. Thus,

$$\begin{aligned} \frac{\partial L_2(\mathbf{U}_1, \Phi_1)}{\partial A_I} &= -\{\mathbf{F}_2\}^{\mathrm{t}} [\mathbf{K}_{uu}]^{-1} \\ &\quad \times \left\{ \frac{\partial [\mathbf{K}_{u\phi}]}{\partial A_I}\{\mathbf{\Phi}_1\} + \frac{\partial [\mathbf{K}_{uu}]}{\partial A_I}\{\mathbf{U}_1\} \right\} \\ &= -\{\mathbf{\Lambda}\}_2^{\mathrm{t}} \left\{ \frac{\partial [\mathbf{K}_{u\phi}]}{\partial A_I}\{\mathbf{\Phi}_1\} + \frac{\partial [\mathbf{K}_{uu}]}{\partial A_I}\{\mathbf{U}_1\} \right\}; \end{aligned} \tag{A.3}$$

$$\text{and} \qquad [\mathbf{K}_{uu}]\{\mathbf{\Lambda}\}_2 = \{\mathbf{F}_2\}. \tag{A.4}$$

Therefore, the sensitivity can be obtained by solving the adjoint problem (see equation (A.4)) and substituting $\{\mathbf{\Lambda}\}_2$ into equation (A.3). Actually, the same expressions are valid for calculating the sensitivity of $L_4(\mathbf{U}_1, \Phi_1)$ by replacing the subscript 2 by 4.

Similarly, the sensitivity of the mean compliance is given by Silva *et al* (2000):

$$\frac{\partial L_3(\mathbf{U}_3, \Phi_3)}{\partial A_I} = -\{\mathbf{\Lambda}\}_3^{\mathrm{t}} \left\{ \frac{\partial [\mathbf{K}_{u\phi}]}{\partial A_I}\{\mathbf{\Phi}_3\} + \frac{\partial [\mathbf{K}_{uu}]}{\partial A_I}\{\mathbf{U}_3\} \right\} \tag{A.5}$$

$$\text{and} \qquad [\mathbf{K}_{uu}]\{\mathbf{\Lambda}\}_3 = \{\mathbf{F}_3\}. \tag{A.6}$$

By means of equation (15), one obtains the derivatives $\partial [\mathbf{K}_{u\phi}] / \partial \rho_{1\mathrm{I}}$ and $\partial [\mathbf{K}_{uu}] / \partial \rho_{1\mathrm{I}}$, which are given by

$$\begin{aligned} \left[\frac{\partial \mathbf{K}_{uu}}{\partial \rho_{1\mathrm{I}}} \right] &= \sum_{e=1}^{\mathrm{NEL}} \int_{\Omega_e} \mathbf{B}_u^{\mathrm{t}} \frac{\partial \mathbf{C}^H}{\partial \rho} \frac{\partial \rho}{\partial \rho_{1\mathrm{I}}} \mathbf{B}_u \, \mathrm{d}\Omega_e \\ &= \sum_{e=1}^{nf} \int_{\Omega_e} \mathbf{B}_u^{\mathrm{t}} \frac{\partial \mathbf{C}^H}{\partial \rho} N_I(\mathbf{x}) \mathbf{B}_u \, \mathrm{d}\Omega_e; \end{aligned} \tag{A.7}$$

$$\left[\frac{\partial \mathbf{K}_{u\phi}}{\partial \rho_{1\mathrm{I}}} \right] = \sum_{e=1}^{nf} \int_{\Omega_e} \mathbf{B}_u^{\mathrm{t}} \frac{\partial \mathbf{e}^H}{\partial \rho} N_I(\mathbf{x}) \mathbf{B}_\phi \, \mathrm{d}\Omega_e \tag{A.8}$$

where the standard finite element definitions of $\mathbf{K}_{uu}$ and $\mathbf{K}_{u\phi}$ are used. The parameter NEL is the total number of finite elements, $\mathbf{B}_u$ is a function of the derivative of shape functions defined in the literature (Cook *et al* 1989), nf is the number of elements connected to node I (that is, the last summation is performed considering only these elements), and $\partial \mathbf{C}^H / \partial \rho_1$ and $\partial \mathbf{e}^H / \partial \rho_1$ can be easily obtained by differentiating equations (8) and (9), respectively. The derivatives $\partial [\mathbf{K}_{u\phi}] / \partial \rho_{2\mathrm{e}}$ and $\partial [\mathbf{K}_{uu}] / \partial \rho_{2\mathrm{e}}$ are

$$\left[\frac{\partial \mathbf{K}_{uu}}{\partial \rho_{2\mathrm{e}}} \right] = 0 \tag{A.9}$$

$$\left[\frac{\partial \mathbf{K}_{u\phi}}{\partial \rho_{2\mathrm{e}}} \right] = \int_{\Omega_e} \mathbf{B}_u^{\mathrm{t}} \frac{\partial \mathbf{e}^H}{\partial \rho_{2\mathrm{e}}} \mathbf{B}_\phi \, \mathrm{d}\Omega_e, \tag{A.10}$$

because only element 'e' depends on the design variable $\rho_{2\mathrm{e}}$.

Appendix B. Nomenclature

List of symbols:

(x, z)	coordinate system
A_I	design variable
$\mathbf{B}_u, \mathbf{B}_\phi$	functions of the derivative of shape functions
$\mathbf{c}^E$	elastic tensor
$\mathbf{C}^H$	elastic tensor for the mixture
$\mathbf{C}_0$	elastic tensor of basic material
$\mathbf{C}_i$	elastic tensor for material type i
d	distributed electrical charge
$\mathbf{D}$	electrical displacement vector
$\mathbf{e}$	piezoelectric tensor
$\mathbf{e}^H$	piezoelectric tensor for the mixture
$\mathbf{e}_i$	piezoelectric tensor for material type i
$\overline{\mathbf{e}}_i$	unit vector
$\mathbf{E}_i$	electrical field associated with load case i
$\mathbf{F}$	nodal mechanical force
$f(.)$	projection function f
$\mathcal{F}$	objective function
$\mathbf{n}$	normal vector
$\mathbf{Q}$	nodal electrical charge
$\{\mathcal{Q}\}$	force and electrical charge vector
$\mathbf{K}_{uu}$	stiffness matrix
$\mathbf{K}_{u\phi}$	piezoelectric matrix
$\mathbf{K}_{\phi\phi}$	dielectric matrix
$[\mathcal{K}]$	system matrix
$L_2(\mathbf{u}_1, \phi_1)$	mean transduction
$L_3(\mathbf{u}_3, \phi_3)$	mean compliance
$L_4(\mathbf{u}_1, \phi_1)$	coupling constraint function
$N_I(\mathbf{x})$	finite element shape function
N_{des}	number of nodes in the design domain
NEL	total number of finite elements
nf	number of elements connected to node I
r_{ij}	distance between nodes i and j
$r_{\min}$	minimum length
S	design domain
$\mathbf{t}$	traction
$\mathbf{u}$	displacement field
u_i and v_i	node i horizontal and vertical displacement, respectively
$\mathbf{U}$	nodal displacements
$\{\mathcal{U}\}$	displacement and electrical degrees of freedom vector
$\mathbf{v}$	virtual displacement
V	space
V_a	space for load case 1
V_b	space for load case 2
V_c	space for load case 3
V_I	finite element volume
$\mathbf{x}$	position coordinate vector
y_n	design variable associated with node n
w	general weight coefficient
W	weight for projection function
β	weight coefficient for coupling constraint function
$\boldsymbol{\epsilon}^S$	dielectric tensor
$\boldsymbol{\varepsilon}(\mathbf{u})$	strain
ϕ	electric potential
ϕ_{ij}	jth potential at the ith node
$\phi_a, \phi_b, \phi_c, \phi_d$	electrical degrees of freedom in the finite element
ϕ_0	applied electrical voltage
$\mathbf{\Phi}$	nodal electric potential vector
$\Gamma_{\mathbf{u}}$	surface of prescribed displacements
Γ_ϕ	surface of prescribed electrical degrees of freedom
$\Gamma_{\mathbf{t}_i}$	surface of applied mechanical traction for load case i
Γ_{d_i}	surface of applied electrical voltage for load case i
φ	virtual electric potential
$\{\mathbf{\Lambda}\}$	auxiliary vector
Θ	volume of design domain
Θ_1	upper-bound volume constraint for material type 1
ρ_1	design variable to describe the type of piezoelectric material
ρ_2	design variable for the polarization (of the piezoelectric material)
$\rho_{1\text{I}}$	nodal design variable related to material distribution
$\rho_{2\text{e}}$	element design variable related to polarization sign
$\boldsymbol{\sigma}$	stress tensor
Ω	domain
Ω_e	element domain
$\nabla\phi$	gradient of electrical potential
∇	gradient operator

References

Almajid A, Taya M and Hudnut S 2001 Analysis of out-of-plane displacement and stress field in a piezocomposite plate with functionally graded microstructure *Int. J. Solids Struct.* **38** 3377–91

Ballato J, Schwartz R and Ballato A 2001 Network formalism for modeling functionally graded piezoelectric plates and stacks *IEEE Trans. Ultrason. Ferroelectr. Freq. Control* **48** 462–76

Bendsøe M P and Kikuchi N 1988 Generating optimal topologies in structural design using a homogenization method *Comput. Methods. Appl. Mech. Eng.* **71** 197–224

Bendsøe M P and Sigmund O 2003 *Topology Optimization—Theory, Methods and Applications* (New York: Springer)

Brady G S, Clauser H R and Vaccari J A 1997 *Materials Handbook* (New York: McGraw-Hill)

Carbonari R C, Silva E C N and Nishiwaki S 2005 Design of piezoelectric multiactuated microtools using topology optimization *Smart Mater. Struct.* **14** 1431–47

Carbonari R C, Silva E C N and Nishiwaki S 2007 Optimum placement of piezoelectric material in piezoactuator design *Smart Mater. Struct.* **16** 207–20

Chen L and Roytburd A L 2007 180° ferroelectric domains as elastic domains *Appl. Phys. Lett.* **90** 102903

Chen Y H, Li T and Ma J 2003 Investigation on the electrophoretic deposition of a FGM piezoelectric monomorph actuator *J. Mater. Sci.* **38** 2803–7

Cook R D, Malkus D S and Plesha M E 1989 *Concepts and Applications of Finite Element Analysis* (New York: Wiley)

Elka E, Elata D and Abramovich H 2004 The electromechanical response of multilayered piezoelectric structures *J. Microelectromech. Syst.* **13** 332–41

Guest J K, Prévost J H and Belytschko T 2004 Achieving minimum length scale in topology optimization using nodal design

variables and projection functions *Int. J. Numer. Methods. Eng.* **61** 238–54
Haertling G H 1994 Rainbow ceramics—a new type of ultra-high-displacement actuator *Am. Ceram. Soc. Bull.* **73** 93–6
Hanson R and Hiebert K 1981 A sparse linear programming subprogram *Technical Report SAND81-0297* (Sandia National Laboratories)
Ikeda T 1996 *Fundamentals of Piezoelectricity* (Oxford: Oxford University Press)
Kim J H and Paulino G H 2002 Isoparametric graded finite elements for nonhomogeneous isotropic and orthotropic materials *ASME J. Appl. Mech.* **69** 502–14
Kögl M and Silva E C N 2005 Topology optimization of smart structures: design of piezoelectric plate and shell actuators *J. Smart Mater. Struct.* **14** 387–99
Lerch R 1990 Simulation of piezoelectric devices by two- and three-dimensional finite elements *IEEE Trans. Ultrason. Ferroelectr. Freq. Control* **37** 233–47
Matsui K and Terada K 2004 Continuous approximation of material distribution for topology optimization *Int. J. Numer. Methods Eng.* **59** 1925–44
Miyamoto Y, Kaysser W A, Rabin B H, Kawasaki A and Ford R G 1999 *Functionally Graded Materials: Design, Processing and Applications* (Dordrecht: Kluwer–Academic)
Naillon M, Coursant R H and Besnier F 1983 Analysis of piezoelectric structures by a finite element method *Acta Eletron.* **25** 341–62
Qiu J, Tani J, Ueno T, Morita T, Takahashi H and Du H 2003 Fabrication and high durability of functionally graded piezoelectric bending actuators *Smart Mater. Struct.* **12** 115–21
Rahmatalla S and Swan C C 2004 A Q4/Q4 continuum structural topology optimization implementation *Struct. Multidiscip. Optim.* **27** 130–5
Shi Z F and Chen Y 2004 Functionally graded piezoelectric cantilever beam under load *Arch. Appl. Mech.* **74** 237–47
Sigmund O 2000 Topology optimization: a tool for the tailoring of structures and materials *Phil. Trans. R. Soc. Lond.* A **358** 211–27
Silva E C N, Nishiwaki S and Kikuchi N 2000 Topology optimization design of flextensional actuators *IEEE Trans. Ultrason. Ferroelectr. Freq. Control* **47** 657–71
Suresh S and Mortensen A 1988 *Fundamentals of Functionally Graded Materials* (London: IOM Communications Ltd.)
Taya M, Almajid A A, Dunn M and Takahashi H 2003 Design of bimorph piezo-composite actuators with functionally graded microstructure *Sensors Actuators* A **107** 248–60
Torquato S 2002 *Random Heterogeneous Materials—Microstructure and Macroscopic Properties* (New York: Springer)
Vanderplaatz G N 1984 *Numerical Optimization Techniques for Engineering Design: with Applications* (New York: McGraw-Hill)
Ying C and Zhifei S 2005 Exact solutions of functionally gradient piezothermoelastic cantilevers and parameter identification *J. Intell. Mater. Syst. Struct.* **16** 531–9
Zhifei S 2002 General solution of a density functionally gradient piezoelectric cantilever and its applications *Smart Mater. Struct.* **11** 122–9
Zhu X H and Meng Z Y 1995 Operational principle, fabrication and displacement characteristics of a functionally gradient piezoelectric ceramic actuator *Sensors Actuators* A **48** 169–76